Vol. **114** (2008) *ACTA PHYSICA POLONICA A* Supplement

Proceedings of the Professor Stefan Mróz Symposium

Resonant Photoemission Study of $4f$ Electrons on the Surface of Semiconductors

B.A. Orłowski*, B.J. Kowalski, M. Pietrzyk and R. Buczko

Institute of Physics, Polish Academy of Sciences
al. Lotników 32/46, 02-668 Warsaw, Poland

The contribution of $4f$ electrons to the electronic structure of the semiconductor clean surface caused by the surface doping of it by rare-earth metal atoms (Eu, Sm) will be presented. The surface doping was performed by the controlled, sequential deposition of the rare-earth metal atoms on the clean surface in UHV conditions (Sm on GaN or CdTe) or by the doping of the layer volume of (EuGd)Te. After each deposition or surface treatment the synchrotron radiation was used to measure *in situ* the resonant photoemission spectra (the Fano type resonance) to study the contribution of $4f$ electrons of divalent and trivalent Sm and Eu ions to the valence band electronic structure of created sample. The first stages of the metal atoms deposition lead to the surface doping. Further metal atoms deposition leads to the growth of the metallic islands on the surface and causes the appearance of the sharp metallic Fermi edge in the energy distribution curves. Proper coverage and annealing of the sample surface with metal atoms leads to the diffusion of the metal atoms into the sample and results in an increase in the crystal doping and decrease in the metallic islands contribution to the measured spectra. As a result, the new electronic structure of the valence band can be created and investigated *in situ*.

PACS numbers: 79.60.Bm, 71.20.Mq, 07.85.–m

1. Introduction

The construction of modern nanostructure elements stimulates the progress in the study of the fundamental parameters of crystalline and electronic structure of the surface and surface region of solids. These studies need, on one hand, properly clean and advanced technology and, on the other hand, proper and advanced control of the change of the parameters of crystalline and electronic structure of nanostructure elements. Large number of the newly obtained results occurs due

*corresponding author; e-mail: orbro@ifpan.edu.pl

to the application of the new experimental methods based on the application of the synchrotron radiation obtained in the synchrotron storage ring [1–7].

The synchrotron radiation — continuous and strong radiation in wide range of energy $h\nu$ starting from microwave and infrared ($h\nu \leq 1$ eV) continued by the visible and ultraviolet (1 eV $\leq h\nu <$ 300 eV) and then soft X-ray ($300 \leq h\nu <$ 10000 eV) up to hard X-ray 100000 eV opens new unexpected possibilities to apply it for study optical and X-ray properties of matter. Continuity of radiation in these range of energy gives the possibility to tune the energy $h\nu$ of obtained radiation to the resonant transitions in the selected atom of the sample material and to selected local structure of it. The experimental equipment collected around the synchrotron storage ring (rich and modern) create an excellent laboratory for optical and X-ray experiments to be performed in so wide range of energy. New scientific techniques are being developed in areas of atomic, molecular, solid state physics, physical chemistry, biophysics, and medicine. Synchrotron came to be the center of interdisciplinary laboratory applying modern optical and X-ray radiation source. As an example the precise measurement of X-ray atomic absorption edges, extended X-ray absorption fine structure (EXAFS) or X-ray absorption near edge structure (XANES) were performed to determine the local structure in the crystals (nearest neighbor distance in e.g. doped crystal or organic compounds). The anomaly strong Fano-type resonance [8–10] correlated to the highly localized transitions $3p^6{-}3d^n$ or $4d^{10}{-}4f^n$ in transition metal [10–20] or rare-earth [20–32] atoms, respectively, were observed and applied for study of electronic structure and contribution of the states of these atoms to the semimagnetic or magnetic semiconductors valence band electronic structure. Continuous, high intensity and tunable light source gives the possibility to study particular resonance transition effects appearing for single isolated atoms as well as for atoms incorporated in the clusters, liquids, volume of the solids or their surface.

The paper presents the application of synchrotron ultraviolet radiation for crystals and layers, their clean surface electronic structure was changed by the selected impurity atoms sequentially deposited and then diffused to the volume of the crystal in the surface region. For some cases the same selected impurities were introduced into the volume of the crystals or layers during the growth technology (modified Bridgman method or molecular beam epitaxy (MBE) method, respectively). Then the selected atoms were deposited on the surface under control of their amount starting from a fractional part of monolayer up to several layers. The sample prepared in this way was annealed by proper thermal treatment to perform the diffusion of adsorbed atoms to the surface region of the crystal or layer. In each step of the sample treatment the change of the electronic structure was investigated *in situ* by resonant photoemission spectroscopy with application of the synchrotron radiation.

Resonant photoemission spectroscopy (RPES) [8–10] is presented in the paper as a good example for application of the tunable ultraviolet light source in

the range of energy from 10 to 200 eV for an electronic structure study of the crystal surface and volume. In this technique the radiation energy $h\nu$ is tuned to the resonant electron transition, e.g. $4d{-}4f$ for rare-earth atoms in the range of the energy region from 100 to 200 eV [7], to excite locally and selectively the electrons in the particular chosen atoms e.g., Sm atoms deposited and diffused to the sample or Eu introduced during MBE growth of the (EuGd)Te layer. For this particular resonant energy the increase in the elements (peaks or structures) of the measured energy distribution curve (EDC) of photoemitted electrons was studied. The increase in these elements in the $h\nu$ region corresponding to the $4d{-}4f$ transition gives the possibility to prescribe the observed peak or structure as corresponding to the contribution of the electrons of this particular atom to the electronic structure in the crystal valence band energy region and to determine the binding energy and structure of this contribution.

RPES will be presented as a tool to determine the contribution of the localized orbital of the electrons $4f$ of the rare-earth metal atoms to the sample valence band electronic structure. The experimental results obtained in the case when the impurity atoms are deposited on the clean surface of the semiconductor compounds can be compared with the case when the impurity atoms are introduced to the volume of the crystal during crystal growth by the modified Bridgman method e.g. (PbRE)Se (RE = rare-earth atoms) [22–27].

2. Photoemission electron spectroscopy

The used illumination of the sample leads to the photoemission of electrons from both the surface and the volume of the sample. The photoelectron energy analyzer, controlled by the computerized electronic system, gives the EDCs of the emitted electrons. The analyzer can measure an angle-integrated EDC or it can measure EDC as a function of the particular take-off angle (angle-resolved EDC, AREDC). In the first case the angle-integrated EDCs determine the electronic structure (the energy dependence of the density of states) while in the second case the angle-resolved EDCs give the possibility to determine the band structure — $E(\boldsymbol{k})$ (where $\boldsymbol{k}$ — electron momentum) dependence for the measured crystal surface. The origin of the measured EDC is illustrated in Fig. 1.

The absorption coefficient of the ultraviolet radiation is in the range of 10^6 cm^{-1}, so the radiation penetrates into the sample to a distance of several hundreds of Å. The escape depth of the electrons leaving the crystal (the distance at which the number of escaping electrons decreases by a fraction of $1/e$) depends strongly on the kinetic energy of the emitted electrons and its value can change from several Å up to several hundreds of Å [1–7]. In a case when the kinetic energy of the escaping electron is about 90 eV, the escape depth reaches a minimum value equal to several Å and in these kinetic energy region the maximum of contribution to the measured EDC of the electrons photoemitted from the surface appears. This region of electron kinetic energy is commonly used to distinguish

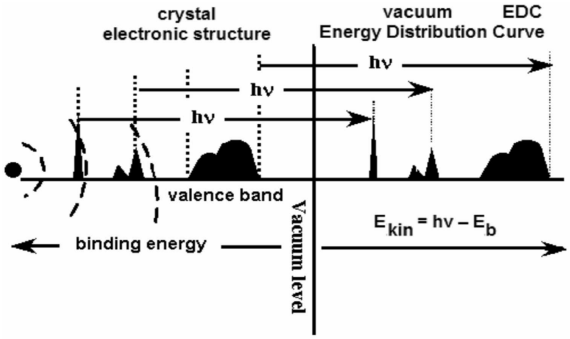

Fig. 1. The model of the EDC creation. The left-hand side of the figure presents the density of the occupied states distribution in the crystal. Radiation of the energy $h\nu$ shifts up the electrons from the electronic occupied bands of the crystal to the free electron states in the vacuum. The electron energy analyzer registers the EDC of escaped from crystal electrons for particular $h\nu$ energy.

surface electronic structure contributions to the measured spectra. If the kinetic energy of escaping electron is far from 90 eV, the continuous and pronounced increase in the escape depth leads to a decrease in the surface electrons contribution relatively to the volume electrons contribution to the measured spectra.

3. Resonant photoemission spectroscopy

Considerable effort has been devoted towards understanding the contribution of the electrons of RE metal ions to the valence band using resonant photoemission experiment. The resonant and non-resonant photoemission processes are illustrated in Fig. 2. Non-resonant photoemission (Fig. 2a) occurs due to direct interaction of $h\nu$ photon with the electron. Resonant photoemission (Fig. 2b) of electron is followed by resonant absorption of $h\nu$ photon and creation of excited state of the atom. Relaxation of the atom leads to the emission of the electron.

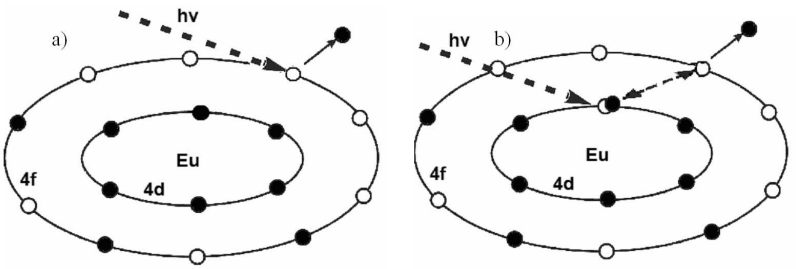

Fig. 2. Illustration of (a) non-resonant photoemission: Eu $4d^{10}4f^7 + h\nu$ = Eu $4d^{10}4f^6 + e$; and (b) resonant Fano-type photoemission: Eu $4d^{10}4f^7 + h\nu$ = [Eu $4d^9 4f^8]^*$ = Eu $4d^{10}4f^6 + e$ (* — excited state).

Application of the tunable energy $h\nu$ radiation source gives a possibility to tune the radiation energy $h\nu$ to the particular resonant electron transition between electron levels in the atom (e.g., $4d{-}4f$ electron transition for Eu: $4d^{10}4f^7 \rightarrow 4d^9 4f^8$). However, even for the single atom not interacting with an environment, the final discrete localized state (Eu:$4d^9 4f^8$) is not the eigenstate of the system. Due to Coulombic configuration interaction the proper final eigenstate is the superposition of the localized (Eu:$4d^9 4f^8$) and delocalized (Eu:$4d^{10}4f^6 + e$) parts. The latter configuration is related to the photoionization of the atom and gives an electron in photoemission. The adjectives localized and delocalized have been used here to underline the fact that in the first case all electrons are localized in the vicinity of the atom and in the second case one of electrons is delocalized (photoemitted). Because the interaction takes place for a broad range of the photoemitted electron energy E, the discrete state (Eu:$4d^{10}4f^7$ configuration) is diluted throughout the final states of the energy continuum. Fano [8] has shown that these final photoionization states for the energies close to the resonance can be represented by the following form: $\Psi_E = \Phi_E \sin \Delta_E + \psi_E \cos \Delta_E$, where ψ_E is the pure delocalized configuration, Φ_E is the localized one modified (dressed) by the admixture of delocalized configurations ψ_E from the energy vicinity. Both parts give the contribution to the photoemitted electron. The phase shift Δ_E as well as the configurations mixing depends on the matrix elements used to ascribe autoionization processes. When energy E passes through the resonance the phase shift Δ_E quickly changes its value by π. As a result, the both parts contribute with different sign below and above the resonance when the amplitude of the optical transition from the ground to the final photoionization state is calculated and the resonant line shape (in optical absorption as well as in the photoemission) is asymmetric. The maximum can be interpreted as related to the photoionization (of $4f$ electrons in Eu case) reinforcement by the possibility of the ($4d^{10}4f^7 \rightarrow 4d^9 4f^8$) transition inside the atom.

The radiation energy tuned to the maximum can be used for the studies of small amount of rare-earth ions in crystals and beside gives the information of the amount of the ions. It provides also the information of the position of $4f$ states against the valence band. The contribution of resonant photoemission can be described by the Fano formula introduced for atomic systems and illustrated by the Fano line shape with the resonant maximum followed by the anti-resonant minimum [8]. The profile of the line can be more complex when the transition metal appears as an impurity in the semiconductor or as a crystal component.

4. Samples and experimental

The investigated samples of (EuGd)Te were grown in home-built MBE machine using effusion cells for Eu, Gd and Te sources in the Institute of Physics, Polish Academy of Sciences in Warsaw [21–24]. The layers were grown on the freshly cleaved in air BaF_2 (cubic structure with lattice constant $a_0 = 6.20$ Å)

(111) surface. The surface was annealed at 560°C in MBE preparation chamber and thin EuTe buffer layer with thickness about 50 nm was deposited. Then the (EuGd)Te layer (rock salt structure with $a_0 = 6.60$ Å) was deposited. After the annealing procedure some of the samples were exposed to air and for photoemission experiment they were cleaned by argon ion sputtering and annealed in preparation chamber of photoemission spectrometer. To avoid this cleaning procedure the other samples were protected by Te amorphous layer (about 100 nm thick) deposited *in situ* in MBE chamber and then exposed to air. For photoemission experiment protected Te layer was removed by annealing of the sample at temperature of about 300°C in UHV conditions and measured *in situ*. The typical thickness of (EuGd)Te layer was in the range of 200–300 nm and the Gd concentration was below 2%. The EuTe isolated sample came to be conducting due to introduction of Gd $5d$ electrons to the conduction band.

The photoelectron spectrometer at the beam line E1 (FLIPPER II monochromator for range of energy 10 eV $< h\nu <$ 200 eV of DORIS storage ring ($h\nu < 100$ keV) at HASYLAB (Hamburg, Germany) was used to obtain the photoemission data presented in this paper. The special convenient feature of this station is the possibility to perform cleaning of the surface *in situ* (Ar ions sputtering and thermal treatment), to deposit particular atoms in UHV conditions and to take the spectra with application of VUV grid monochromator (FLIPPER II) with low intensity of the second order of $h\nu$ lines. Controlled set of EDCs was taken after each treatment of the surface. The photon energy range was chosen between 120 eV and 160 eV to cover the region of $4d{-}4f$ Fano resonances both for Eu^{2+} and Eu^{3+} ions. The region of EDCs was recorded from the valence band edge down to the Te $4d$ (41 eV) core level. All spectra were normalized taking into account the photon flux and the secondary electron scattering was subtracted. One of the investigation goals was to determine the optimal thermal annealing conditions for (EuGd)Te protected by Te layer. The sputtering and annealing removes the Te layer and simultaneously the measured spectra of electronic structure of (EuGd)Te without Te layer can be measured. The investigated samples were annealed in two stages: (1) at the different temperatures between 240°C and 350°C during 3 h; and (2) at $T = 320$°C during different time interval: 21 h plus 10 h plus 10 h. After each annealing process the photoemission spectra were measured to compare the influence of annealing on the height and sharpness of Eu^{2+} and Eu^{3+} peaks [24].

As a result of the first type of annealing we can measure the sufficient contributions of both Eu^{2+} $4f$ and Eu^{3+} $4f$ electrons. For the higher annealing temperatures the concentration ratio Eu^{3+}/Eu^{2+} decreases but unfortunately the Eu^{3+} peak remains quite strong. Besides, the peak corresponding to Te $4d$ was broad and without visible spin–orbit splitting. It indicates that the crystal structure of (EuGd)Te does not improve. In Fig. 3a the set of EDCs is presented in the range of energies between 130 and 160 eV. This range of $h\nu$ energy corresponds to the Fano resonant energy region for Eu $4d{-}4f$ transition. In this stage of the

surface preparation the sets of EDCs corresponding to the Eu $4d-4f$ resonance were observed for divalent as well as for trivalent Eu ions. The height of peak corresponding to the Eu^{2+} $4f$ located at the edge of the valence band grows in the part of lower $h\nu$ energies, while for Eu^{3+} $4f$ located in the valence band (5–10 eV region) it grows in the upper range of $h\nu$ energies. After the next annealing (41 h at 320°C) the electronic structure (Fig. 3b) was remarkably improved and well approached the structure of crystalline and stoichiometric EuTe. The Eu^{2+} peaks became sharp and narrow and the Eu^{3+}/Eu^{2+} concentration ratio became negligible small. Furthermore, the Te $4d$ peak became also narrow and its spin–orbit splitting became more distinctly visible [21, 24]. In this way the proper conditions for annealing of the layer to obtain clean surface and crystalline layer with proper stoichiometry were found.

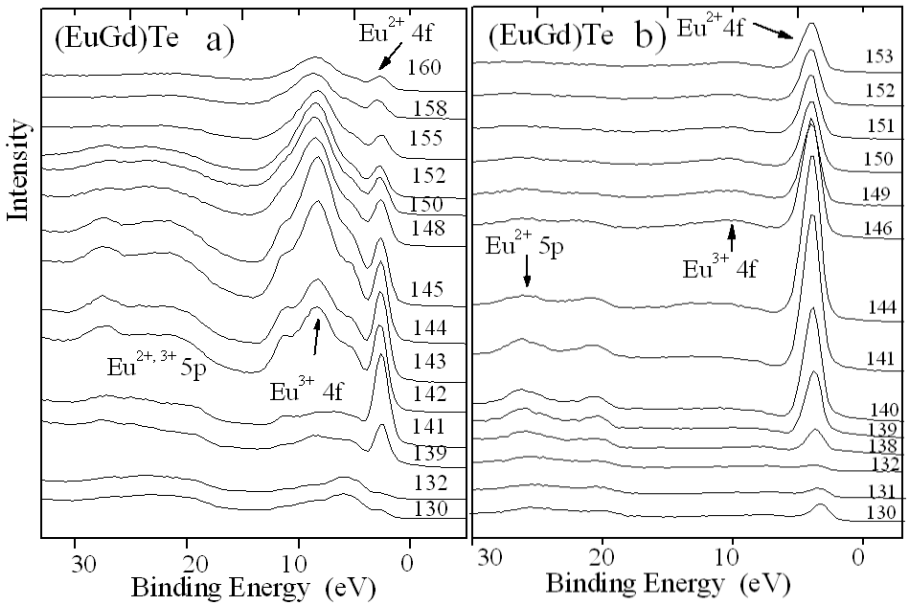

Fig. 3. Set of EDCs of (EuGd)Te layer after (a) sputtering of Te protection layer and partial annealing and (b) additional long annealing for 41 h in 320°C.

Let us take as an example of rare-earth atoms deposited on the surface of semiconductors the atoms of Sm on CdTe (100) and GaN (000$\underline{1}$) surfaces. Cleaning of the samples was performed by argon ion sputtering ($E = 600$ eV, $t = 1$ h) and by annealing in the range of 260°C or 500°C for CdTe and GaN, respectively. The Sm atoms were deposited from the Knudsen cell calibrated with quartz microbalance. The deposition was performed on substrate of room temperature. The cadmium and gadolinium are characterized by the valence 2+ and 3+, respectively. It can be expected that the samarium substituting the cadmium or gadolinium will prefer their valences.

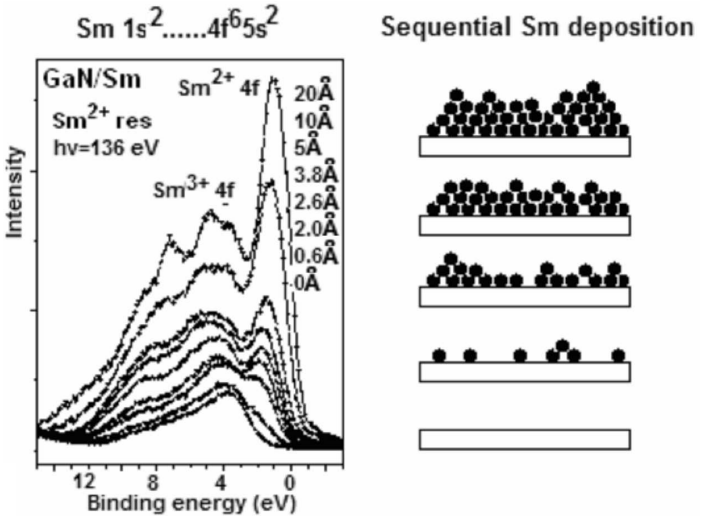

Fig. 4. The set of EDCs obtained for sequentially deposited Sm atoms on GaN (000$\underline{1}$) surface obtained for radiation energy equal to the Fano resonant for divalent Sm ions $h\nu = 136$ eV.

In Fig. 4 the set of EDCs corresponding to the sequentially deposited Sm atoms on GaN(000$\underline{1}$) surface measured for the photon energy corresponding to the Sm $4d{-}4f$ transition Fano resonance for divalent Sm ion is presented. The curve at the bottom corresponds to the clean GaN (000$\underline{1}$) surface. The divalent and trivalent Sm $4f$ multiplet structures contribute to the obtained spectra. The first peak located at the top part of the valence band corresponds to the divalent Sm $4f$ electrons multiplets while the structure located in the region of binding energy 5–10 eV corresponds to the trivalent Sm $4f$ electrons multiplets [31, 32]. In first stages of Sm deposition up to 5 ML (monolayers) the contribution of divalent and trivalent multiplets appears. As the used radiation energy 136 eV is resonant for divalent Sm we can conclude that in these stage of deposition the concentration of trivalent Sm dominates in the deposited atoms. In the next stages of Sm deposition the divalent contribution dominates. In Fig. 5 the set of EDCs measured for the photon energy corresponding to the Sm $4d{-}4f$ transition Fano resonance for trivalent Sm ion is presented. In these case the trivalent Sm $4f$ multiplets contribution dominates in the whole range of Sm atoms deposition. For the same sample the difference between curves presented in Fig. 4 and Fig. 5 is remarkable. In Fig. 4 the peaks corresponding to the $4f$ electrons of Sm divalent ions dominate ($h\nu = 136$ eV corresponds to the Fano resonant of divalent Sm ion), while in Fig. 5 the peaks corresponding to the $4f$ electrons of Sm trivalent ions dominate ($h\nu = 141$ eV corresponds to the Fano resonant of trivalent Sm ion).

In Fig. 6a, b the sets of EDCs measured for the Sm atoms deposited on GaN and CdTe are presented. The cations of these chemical compounds have the

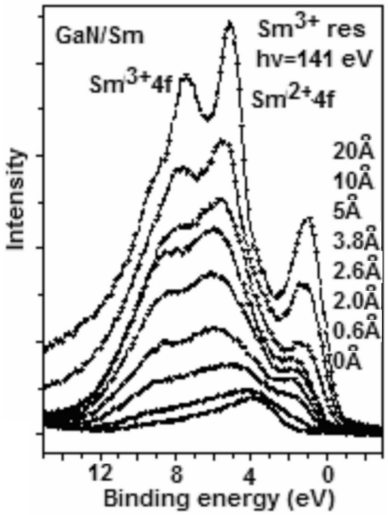

Fig. 5. The set of EDCs obtained for the set of sequentially deposited films of Sm atoms on GaN (000$\underline{1}$) surface obtained for radiation energy $h\nu = 141$ eV, resonant for trivalent Sm ions, to compare with Fig. 4.

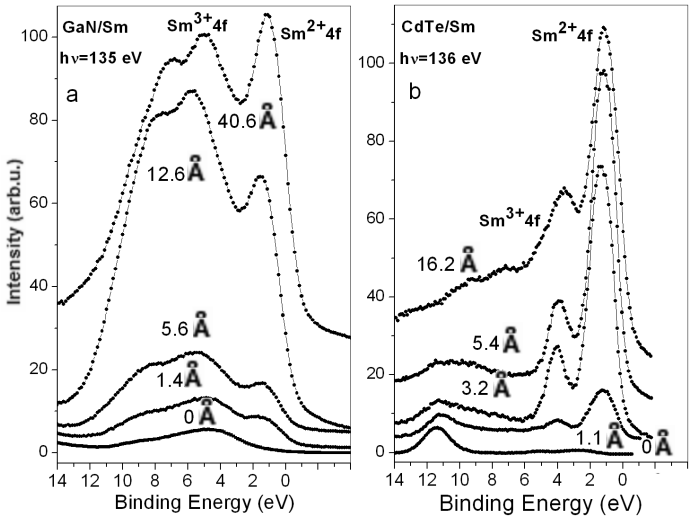

Fig. 6. The set of EDCs obtained for sequentially deposited Sm atoms on (a) GaN (000$\underline{1}$) and (b) CdTe (100).

different valence — trivalent Gd and divalent Cd. In Fig. 6a the radiation energy $h\nu = 135$ eV is more convenient for magnification of divalence than trivalence as it is close to the divalent Sm Fano resonance while it is far from trivalent Sm energy resonance. Even so, trivalent Sm contribution dominates the divalent contribution in the region of coverage up to 4.5 ML. Up to the range of coverage 4.5 ML the

trivalence of the substrate cation Ga decides on Sm trivalence on the surface. The opposite situation is in Fig. 6b where divalent Cd is in the CdTe substrate. In the case, for deposited Sm atoms divalent Sm dominates in the whole region of the amount of deposition. Trivalent Sm contribution is very small and appears as a two-peaks structure for deposited Sm as much as 9 ML.

5. Summary and conclusions

Synchrotron storage ring is an excellent source of radiation to use it as the continuous tunable light source for the Fano type resonant photoemission spectroscopy. Applying these spectroscopy the contribution of $4f$ electrons of divalent and trivalent Sm and Eu ions to the energy region of the valence band of semiconductor was experimentally recognized. The strong correlation effect of $4f$ electrons leads to the remarkable differences of the contribution for divalent and trivalent ions.

For Sm atoms deposited on the CdTe or GaN surface the divalent and trivalent deposited ions exist. The ratio of the concentration of trivalent and divalent ions changes with the amount of deposited atoms and with the thermal treatment of the covered sample. In the first stages of Sm deposition the divalent ions concentration dominates in the crystals with the divalent cations like EuTe and CdTe and trivalent one dominates in the crystals with trivalent cations like GaN. High chemical reactivity of Sm and Eu leads to the reduction of substrate cations and to creation of complex chemical compounds and alloys e.g. Sm with Ga [32]. Annealing of the (EuGd)Te covered with Te leads to the decrease in trivalent Eu ions concentration and to the creation of good crystalline (EuGd)Te material with divalent Eu ions.

Acknowledgments

This work was supported in part within: MSHE of Poland research projects DESY/68/2007 and grant N202 101 31/0749 as well as by the European Community under contract RII3-CT-2004-506008 (IA-SFS).

References

[1] D.E. Estman, Y. Farge, *Handbook of Synchrotron Radiation*, Vols. 1–4, North-Holland, Amsterdam 1983–1991.

[2] *Introduction to Synchrotron Radiation*, Ed. G. Margaritondo, Oxford University Press, New York 1988.

[3] *Application of Synchrotron Radiation*, Eds. C.R.A. Catlow, G.N. Greaves, Blackie, London 1990.

[4] L. Ley, M. Cardona, *Photoemission in Solids I and II, Topics in Applied Physics*, Vols. 26/27, Springer, Berlin 1979.

[5] *Photoelectron Spectroscopy*, Ed. M. Cardona, *Springer Series in Solid-State Science*, Vol. 82, Springer, Berlin 1996.

[6] *Physical methods of research in biology, medicine and environment protection*, Eds. A.Z. Hrynkiewicz, E. Rokita, Wydawnictwo Naukowe PWN, Warszawa 1999 (in Polish).

[7] B.A. Orlowski, B.J. Kowalski, E. Guziewicz, K. Szamota-Sadowska, N. Barrett, C. Guillot, R.L. Johnson, J. Ghijsen, *Prog. Surf. Sci.* **67**, 323 (2001).

[8] U. Fano, *Phys. Rev.* **124**, 1866 (1961).

[9] B. Sonntag, P. Zimmerman, *Rep. Prog. Phys.* **55**, 911 (1992).

[10] L.C. Devis, *Phys. Rev. B* **25**, 2912 (1989); R.J. Lad, V.E. Henrich, *Phys. Rev. B* **39**, 13478 (1989).

[11] L. Ley, M. Taniguchi, J. Ghijsen, R.L. Johnson, A. Fujimori, *Phys. Rev. B* **35**, 2839 (1987).

[12] M. Taniguchi, Y. Ueda, I. Morisda, Y. Muashita, T. Ohita, I. Souma, Y. Oka, *Phys. Rev. B* **41**, 3069 (1990).

[13] B.A. Orlowski, E. Guziewicz, B.J. Kowalski, N. Barrett, R. Belkhou, D. Radosavkic, D. Martinotti, C. Guillot, J.P. Lacharme, C.A. Sebenne, *Appl. Surf. Sci.* **123/124**, 631 (1998).

[14] E. Guziewicz, B.J. Kowalski, K. Szamota-Sadowska, B.A. Orlowski, J. Masek, R.L. Johnson, *J. Alloys Comp.* **286**, 137 (1999).

[15] E. Guziewicz, B.J. Kowalski, B.A. Orlowski, J. Ghijsen, You Li-Ming, R.L. Johnson, *J. Electron Spectrosc. Relat. Phenom.* **88-91**, 321 (1998).

[16] D.A. Shirley, *Phys. Rev. B* **12**, 4709 (1972).

[17] B.A. Orlowski, B.J. Kowalski, E. Guziewicz, K. Szamota-Sadowska, *Acta Phys. Pol. B* **30**, 2097 (1999).

[18] S. Senba, K. Fujimoto, H. Sato, Y. Fukuma, N. Nakatake, M. Arita, K. Tsuji, H. Asada, T. Kayanagi, H. Namatame, M. Taniguchi, *J. Electron Spectrosc. Relat. Phenom.* **114-147**, 629 (2005).

[19] M.A. Pietrzyk, B.J. Kowalski, B.A. Orlowski, W. Knoff, V. Osinniy, I.A. Kowalik, T. Story, R.L. Johnson, *Acta Phys. Pol. A* **112**, 275 (2007).

[20] B.J. Kowalski, M.A. Pietrzyk, B.A. Orlowski, P. Dziawa, V. Osinniy, J. Pelka, W. Dobrowolski, V.E. Slynko, E.I. Slynko, R.L. Johnson, *J. Electron Spectrosc. Relat. Phenom.* **156**, 315 (2007).

[21] B.A. Orlowski, B.J. Kowalski, M. Pietrzyk, S. Mickievicius, V. Osinniy, P. Dziawa, T. Story, W. Drube, R.L. Johnson, *J. Electronom. Spectrosc. Relat. Phenom.* **156**, 315 (2007).

[22] B.A. Orlowski, P. Dziawa, B. Kowalski, I. Kowalik, M. Pietrzyk, V. Osinniy, T. Story, S. Mickievicius, R. Johnson, *Appl. Surf. Sci.* **252**, 5379 (2006).

[23] V. Osinniy, B.A. Orlowski, P. Dziawa, B.J. Kowalski, M. Pietrzyk, B. Taliashvili, S. Mickievicius, T. Story, R.L. Johnson, *Bull. Polish Synchr. Rad. Soc.* **5**, 213 (2006) (in Polish).

[24] P. Dziawa, B.A. Orlowski, V. Osinniy, M. Pietrzyk, M. Taliashvili, T. Story, R.L. Story, *Mater. Sci.* **25**, 377 (2007).

[25] B.J. Kowalski, E. Guziewicz, B.A. Orlowski, J. Ghijsen, R.L. Johnson, in: *Proc. Fifth National Symp. on Synchrotron Radiation Users*, Eds. M. Lefeld-Sosnowska, J. Gronkowski, Uniwersytet Warszawski, Warszawa 1999, p. 89.

[26] B.J. Kowalski, Z. Golacki, E. Guziewicz, A. Kozanecki, B.A. Orlowski, J. Ghijsen, R.L. Johnson, *J. Alloys Comp.* **286**, 121 (1999).

[27] B.J. Kowalski, Z. Golacki, E. Guziewicz, B.A. Orlowski, J. Ghijsen, R.L. Johnson, in: *Proc. 11th Int. Conf. on Ternary and Multinary Comp., Salford (UK), Conference Series 152G, 1997*, Institute of Physics, Bristol 1998, p. 885.

[28] B.J. Kowalski, J. Ghijsen, Z. Golacki, E. Guziewicz, T. Story, M. Arciszewska, B.A. Orlowski, R.L. Johnson, *J. Electron Spectrosc. Relat. Phenom.* **88-90**, 327 (1998).

[29] W. Burian, J. Szade, T. O'Keevan, Z. Celiński, *Phys. Status Solidi B* **241**, 15 (2004).

[30] B.A. Orlowski, B.J. Kowalski, E. Guziewicz, K. Szamota-Sadowska, *Acta Phys. Pol. B* **30**, 2097 (1999).

[31] E. Guziewicz, B.A. Orlowski, B.J. Kowalski, I. Grzegory, S. Porowski, *Appl. Surf. Sci.* **190**, 356 (2002).

[32] E. Guziewicz, B.J. Kowalski, B.A. Orlowski, A. Szczepanska, Z. Golacki, I. Grzegory, S. Porowski, R.L. Johnson, I.A. Kowalik, *Surf. Sci.* **551**, 132 (2004).